arXiv:cond-mat/0506501v1 [cond-mat.stat-mech] 20 Jun 2005

Transient cavities and the excess chemical potentials of hard-spheroid solutes in dipolar hard sphere solvents

Philip J. Camp*
School of Chemistry, University of Edinburgh, West Mains Road, Edinburgh EH9 3JJ, United Kingdom
(Dated: February 2, 2008)

Monte Carlo computer simulations are used to study transient cavities and the solvation of hard-spheroid solutes in dipolar hard sphere solvents. The probability distribution of spheroidal cavities in the solvent is shown to be well described by a Gaussian function, and the variations of fit parameters with cavity elongation and solvent properties are analyzed. The excess chemical potentials of hard-spheroid solutes with aspect ratios x in the range $1/5 \leq x \leq 5$, and with volumes between one and twenty times that of a solvent molecule, are presented. It is shown that for a given molecular volume and solvent dipole moment (or temperature) a spherical solute has the lowest excess chemical potential and hence the highest solubility, while a prolate solute with aspect ratio x should be more soluble than an oblate solute with aspect ratio $1/x$. For a given solute molecule, the excess chemical potential increases with increasing temperature; this same trend is observed in the case of hydrophobic solvation. To help interpret the simulation results, comparison is made with a scaled-particle theory that requires prior knowledge of a solute-solvent interfacial tension and the pure-solvent equation of state, which parameters are obtained from simulation results for spherical solutes. The theory shows excellent agreement with simulation results over the whole range of solute elongations considered.

I. INTRODUCTION

The solvation of solutes in simple polar solvents is of importance in almost all areas of chemistry and biochemistry. The way in which solvent molecules are ordered (or not) around solute molecules can confer all manner of interesting and useful phenomena upon the solution, including catalytic activity, preferential solvation in solute mixtures, microphase formation, and self-assembly. Some of the most important - and complex - solvation phenomena occur in aqueous solutions of hydrophobic solutes. Hydrophobic solvation is characterized by negative energy and entropy changes accompanying the insertion of hydrophobic solutes in to aqueous phases. One contribution to the energy change is from the ever-present attractive dispersion interactions that operate between all species, but the dominant contribution is from the specific solvent-solvent interactions facilitated by a reorganization (ordering) of the solvent molecules around each solute molecule; this latter effect also gives rise to the negative entropy change. As a result of these changes in energy and entropy, the solubility of a hydrophobic solute in aqueous solution decreases with increasing temperature over quite a wide temperature range; in the case of methane in water the solubility reaches a minimum at $T \simeq 350$ K. The hydrophobic attraction between hydrophobic solutes in aqueous solution is an effective interaction arising from the fact that favorable solvent-solvent interactions are maximized when the solute molecules are in close proximity with one another, as opposed to being completely surrounded by solvent. For a recent discussion of these concepts, and references to the enormous literature in this area, see Ref. 1.

Considerable effort has been directed toward understanding the nature of solvation in aqueous solutions, especially as compared to that in simple non-aqueous solvents. For example, inert gases are less soluble in water than they are in non-aqueous molecular liquids.[2,3,4] Sophisticated molecular theories have been proposed specifically for hydrophobic solvation and attraction.[5,6,7] It was pointed out that the distribution of transient cavities in the pure solvent could be used to characterize such effects as hydrophobic solvation.[8,9] In the early 1990's, computer simulations were used to characterize the transient cavities in a range of molecular liquids.[10,11] This was achieved by calculating the probability of finding a spherical solute-sized cavity in the solvent. It was found that although water has a larger free volume – or alternatively, a smaller effective packing fraction – than do non-aqueous solvents, that free volume is distributed throughout smaller cavities. Moreover, non-aqueous solvents exhibit a greater ability to redistribute free volume in order to accommodate large solute species. Such considerations are of fundamental importance in understanding the hydrophobic interaction and all of its manifestations in biochemistry, nanoscale systems, and materials chemistry.

This very brief discussion highlights the value of understanding the molecular-scale cavity structure in the pure solvents before one proceeds to consider specific solvent-solute systems. In Ref. 9 it was suggested that such investigations could be extended to non-spherical cavities and solutes. Simulation studies of this type have been carried out for various hard-core solute/solvent systems[12,13,14,15,16,17] but we are not aware of any systematic comparison between rod-like and disk-like solutes. The current work is therefore concerned with transient non-spherical cavities and the solvation of non-spherical solutes in model polar solvents. For simplicity, we consider hard-spheroid solutes (or uniaxial hard ellipsoids) in a solvent made up of dipolar hard spheres (DHSs). The DHS system is the simplest model of a po-

lar liquid, and is of considerable intrinsic interest owing to its complex phase behavior.[18,19,20,21,22,23,24,25,26] In particular, the low-temperature properties of the DHS fluid are dominated by the association of particles in 'nose-to-tail' conformations giving rise to chains and rings at low densities, and extended networks at intermediate densities.[18,20,22] Therefore, the DHS system is an interesting example of a fluid that should exhibit large transient cavities as compared to non-polar hard-sphere fluids at the same density. We use Monte Carlo (MC) computer simulations to study the size distributions of prolate (rod-like) and oblate (disk-like) spheroidal cavities in DHS fluids, and relate these distributions to the excess chemical potentials of hard-spheroid solutes. This allows an examination of the role of solute shape, as well as solute volume, on the solubilities of non-polar solutes in polar fluids. Following earlier simulation studies of this type, we compare our calculations with a scaled-particle theory (SPT) which describes the reversible work for insertion and subsequent growth of a single solute molecule in to a solvent.

This article is organized as follows. In Section II we describe the solute and solvent models, the SPT as applied to the model system, and the computer simulation methods employed in this work. Results are presented in Section III, and Section IV concludes the paper.

II. MODEL AND METHODS

A. Model

The DHS solvent consists of hard spheres with diameter σ, each carrying a central dipole moment $\boldsymbol{\mu}$. For two spheres with separation vector $\boldsymbol{r}$, the pair potential energy is

$$u(\boldsymbol{r},\boldsymbol{\mu}_1,\boldsymbol{\mu}_2) = \begin{cases} \infty & r<\sigma \\ \frac{(\boldsymbol{\mu}_1\cdot\boldsymbol{\mu}_2)}{4\pi\epsilon_0 r^3} - \frac{3(\boldsymbol{\mu}_1\cdot\boldsymbol{r})(\boldsymbol{\mu}_2\cdot\boldsymbol{r})}{4\pi\epsilon_0 r^5} & r\geq\sigma \end{cases} \quad (1)$$

where $r=|\boldsymbol{r}|$ and ϵ_0 is the vacuum dielectric permitivity. Thermodynamic parameters of the DHS system are expressed in dimensionless form as follows: the reduced number density $\rho^* = N\sigma^3/V$, where N is the number of particles in a volume V; the reduced dipole moment $\mu^* = \sqrt{\mu^2/4\pi\epsilon_0 k_B T\sigma^3}$, where k_B is Boltzmann's constant, and T is the temperature; the reduced temperature $T^* = (1/\mu^*)^2$. Throughout the rest of the paper, the DHSs will be referred to as component '1'.

We will compute the probability of finding a spheroidal cavity in the DHS fluid centered at a randomly selected point in the system, and hence obtain the excess chemical potentials of hard-spheroid solutes. The solute will be referred to as component '2' of the resulting solution. With the spheroid radial semi-axes denoted by a, and the polar semi-axis by c, the elongation of the spheroid is given by $x = c/a$. The fundamental measures of the spheroid will be required in Section II C, and are therefore recorded in Table I for reference.

B. Thermodynamics

Of central interest in this paper is the excess chemical potential, $\Delta\mu_2$, of hard-spheroid solutes in DHS solvents at low concentrations where solute-solute interactions can be ignored. $\Delta\mu_2$ can be related to the solubility of the solute in a variety of situations, but to provide a concrete example consider the transfer of a solute molecule from an ideal gas to an initially pure solvent (or an extremely dilute solution) such that the volumes of the gas and the solvent separately remain constant. Thermal equilibrium between the gas and the solution is assumed. The chemical potential of the solute in the ideal gas is equal to

$$\mu_2^{\text{vap}} = k_B T \ln \rho_2^{\text{vap}} \mathcal{V} \quad (2)$$

where ρ_2^{vap} is the number density of solutes in the gas phase, and $\mathcal{V}$ is the de Broglie thermal volume of the solute. The chemical potential of solute molecules in solution (in the absence of solute-solute interactions) is written

$$\mu_2 = k_B T \ln \rho_2 \mathcal{V} + \Delta\mu_2 \quad (3)$$

where ρ_2 is the number density of solutes in the solution. When the solute is at chemical equilibrium the chemical potentials of the solute in both phases are equal, and from the mass-action law the associated partition coefficient can be defined as

$$K \equiv \frac{\rho_2}{\rho_2^{\text{vap}}} = \exp\left(-\beta\Delta\mu_2\right). \quad (4)$$

where $\beta = 1/k_B T$. The temperature dependence of the partition coefficient yields information on the energetic and entropic contributions to $\beta\Delta\mu_2$. For transfer under conditions of constant volume the relevant expressions are

$$\Delta u_2 = k_B T^2 \frac{\partial \ln K}{\partial T} \quad (5)$$

for the energy, and

$$\Delta s_2 = k_B \frac{\partial (T \ln K)}{\partial T} \quad (6)$$

for the entropy, where all differentiations are carried out with gas volume, solvent volume, and number of solvent molecules held constant. Widom *et al.* have provided full details of analogous expressions for transfer under conditions of constant pressure, and the physical situations to which Eqs. (5) and (6) are applicable.[1,27]

C. Scaled particle theory

We note that there are several theories of hard solute/solvent systems that rely on representing non-spherical components by spherical particles with effective

TABLE I: Mean radius of curvature, surface area, and volume for prolate and oblate spheroids with radial semi-axis a, polar semi-axis c, and elongation $x = c/a$.

		Prolate ($x > 1$)	Oblate ($x < 1$)
Eccentricity	ϵ	$\sqrt{1 - x^{-2}}$	$\sqrt{1 - x^2}$
Mean radius of curvature	R_2	$\frac{c}{2}\left[1 + \frac{1-\epsilon^2}{2\epsilon}\ln\left(\frac{1+\epsilon}{1-\epsilon}\right)\right]$	$\frac{c}{2}\left[1 + \frac{\arcsin\epsilon}{\epsilon\sqrt{1-\epsilon^2}}\right]$
Surface area	S_2	$2\pi a^2\left[1 + \frac{\arcsin\epsilon}{\epsilon\sqrt{1-\epsilon^2}}\right]$	$2\pi a^2\left[1 + \frac{1-\epsilon^2}{2\epsilon}\ln\left(\frac{1+\epsilon}{1-\epsilon}\right)\right]$
Volume	V_2	$\frac{4}{3}\pi a^2 c$	$\frac{4}{3}\pi a^2 c$

radii;[12,13,14,15,16,17] the resulting effective hard-sphere mixture is then described by accurate semi-empirical formulae, such as the Boublik-Monsoori-Carnahan-Starling-Leland equation of state.[28,29] In this work, we will show that the variations of $\Delta\mu_2$ with solute size and shape can be described most intuitively within a simple version of SPT.[30] The excess chemical potential of a single hard spheroid with radial semi-axis a and polar semi-axis c is equal to the reversible work required to insert a point particle in to the solvent, and then to grow the point particle to full size. Consider, then, a scaled spheroid with radial and polar semi-axes equal to λa and λc, respectively, with $\lambda = 0$ corresponding to the point particle, and $\lambda = 1$ to the full-sized particle. For hard-particle solutes and solvents, the Widom formula relates the excess chemical potential for the solute at reciprocal temperature $\beta = 1/k_BT$ to the probability, P, of inserting a solute at random in to the solution without incurring any overlaps:[31]

$$\beta\Delta\mu_2 = -\ln P. \tag{7}$$

In the spirit of SPT, we will interpolate between results that are correct in the limits $\lambda = 0$ and $\lambda = \infty$ to obtain a result for $\lambda = 1$. When λ is small, the chemical potential of the scaled spheroid is related to the free volume in the solvent, i.e.

$$\beta\Delta\mu_2 \approx -\ln\left[\frac{V - NV_{\rm ex}(\lambda)}{V}\right] \tag{8}$$

where $V_{\rm ex}(\lambda)$ is the excluded volume of the scaled spheroid and a single solvent molecule. Obviously, this is only correct when the solute is sufficiently small that it can only be in the vicinity of one solvent molecule at any given time. The sphere-scaled spheroid excluded volume is given by the following expression due to Kihara:[32]

$$V_{\rm ex}(\lambda) = V_1 + \lambda S_1 R_2 + \lambda^2 R_1 S_2 + \lambda^3 V_2 \tag{9}$$

The fundamental measures for spheroids are given in Table I; for DHSs the measures are $R_1 = \sigma/2$, $S_1 = \pi\sigma^2$, $V_1 = \pi\sigma^3/6$. In the other extreme, $\lambda \to \infty$, the reversible work for inserting the solute particle is dominated by the work done against the pressure, p, of the solvent, and the (normally positive) contribution to the free energy arising from the interface between the solute molecule and the solvent. In this case the excess chemical potential is

$$\beta\Delta\mu_2 \approx \frac{\lambda^2\gamma S_2}{k_BT} + \frac{\lambda^3 pV_2}{k_BT} \tag{10}$$

where γ is the solute-solvent interfacial tension. We now approximate the excess chemical potential of a full-sized solute molecule with a cubic function of λ: the terms up to order λ are obtained by Taylor expansion of the combination of (8) and (9); and the terms in λ^2 and λ^3 are taken from (10). Finally, we set $\lambda = 1$ (corresponding to the full-sized solute molecule) which yields

$$\beta\Delta\mu_2 = -\ln(1-\eta) + \frac{6\eta}{1-\eta}\left(\frac{R_2}{\sigma}\right) + \frac{\gamma S_2}{k_BT} + \frac{pV_2}{k_BT} \tag{11}$$

where $\eta = \rho V_1$ is the packing fraction of the pure solvent. The first term in (11) arises from the fact that the probability of inserting a point particle in to the solvent without overlap is equal to $(1 - \eta)$. (The surface term proportional to S_2 can also contain an additional curvature contribution[33] but it will be explained below that this is unnecessary in the current application.) The pressure and solute-solvent interfacial tension will be determined from computer simulations which we describe in the next section.

D. Computer simulations

Canonical (NVT) MC simulations of $N = 500$ DHSs were carried out in a cubic simulation cell with periodic boundary conditions applied.[34] The long-range dipolar interaction was handled using the Ewald summation with conducting boundary conditions. One MC cycle consisted of one trial translation and one trial rotation per molecule, on average. Run lengths after equilibration consisted of $\mathcal{O}(10^5)$ MC cycles. The respective maximum displacements for translational and rotational moves were adjusted to give acceptance rates of 20%.

To characterize the cavity structure in the DHS fluid, a test particle was inserted in to the simulation cell with randomly selected position and orientation. For a given elongation, the maximum possible spheroid radial semi-axis, a_m, that would not result in any particle overlaps was determined. This procedure was repeated 500 times

every 20 MC cycles, and a histogram of a_m was accumulated to yield a cavity function $Q(a_m)$, the integral of which is

$$\int_0^\infty Q(a_m)da_m = 1 - \eta. \tag{12}$$

In addition, the excess chemical potentials $\beta\Delta\mu_2 = -\ln P(a)$ were determined using (7) and the fact that for a given test-particle insertion, all spheroids with the same elongation and $a \leq a_m$ would be accommodated in the solvent without overlap. $P(a)$ and $Q(a_m)$ are related because the probability of successfully inserting a test particle with radial semi-axis a is equal to the likelihood of there being a cavity that can accommodate a particle with radial semi-axis of at least that size,[10] i.e.

$$P(a) = \int_a^\infty Q(a_m)da_m = 1 - \eta - \int_0^a Q(a_m)da_m. \tag{13}$$

As will be explained in Section III B, MC simulation results were used to parametrize the SPT expression (11). The pressure in the DHS fluid was determined using the virial equation,[35]

$$\frac{p}{\rho k_B T} = 1 + \frac{2}{3}\pi\rho\sigma^3 g(\sigma) + \frac{U}{Nk_BT} \tag{14}$$

where $g(\sigma)$ is the radial distribution function, $g(r)$, at contact, and U is the dipolar configurational energy. The second term in (14) represents the hard-core contribution to the equation of state; $g(\sigma)$ was estimated by extrapolating $g(r)$ to contact using a $[2,2]$ Padé approximant.

III. RESULTS

The DHS fluid was studied with reduced dipole moments $\mu^* = 0$ (hard spheres), $\mu^* = 1$, and $\mu^* = 2$, corresponding to reduced temperatures of $T^* = \infty$, $T^* = 1$, and $T^* = 0.25$, respectively. The number densities considered were $\rho^* = 0.2$, $\rho^* = 0.5$, and $\rho^* = 0.8$. (For water under ambient conditions, $\mu^* \sim 2$ and $\rho^* \sim 0.9$; rough estimates of the parameters for liquid ammonia are $\mu^* \sim 1$ and $\rho^* \sim 0.8$.) Hard-spheroid solute particles were considered with elongations in the range $1/5 \leq x \leq 5$, and with a range of molecular volumes up to $20V_1$, depending on the density; at higher densities the probability of inserting a large solute particle in to the solvent without overlap becomes too small to enable an accurate evaluation of (7).

A. Cavity distributions and molecular structure

In Fig. 1 we show the cavity distributions, $Q(a_m)$, for spheroidal cavities in a DHS solvent with $\rho^* = 0.2$ and $\mu^* = 2$. Results are presented for spheroids with elongations of $x = 1/5$ (oblate), $x = 1$ (spherical), and $x = 5$ (prolate). The distributions are well described by the Gaussian function

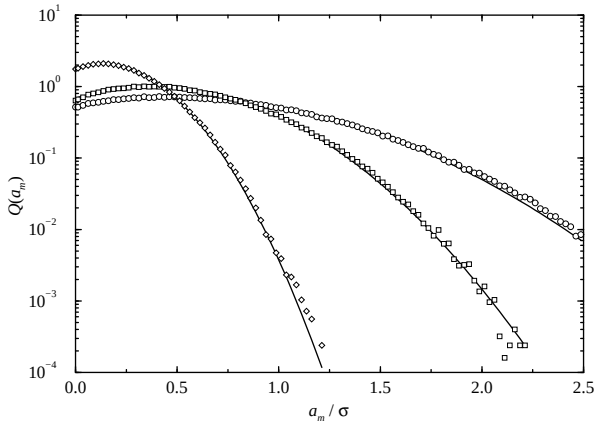

FIG. 1: Linear-log plot of the cavity distribution functions, $Q(a_m)$, for spheroidal cavities of radial semi-axis a and elongation x in a DHS solvent with $\rho^* = 0.2$ and $\mu^* = 2$: $x = 1/5$ (circles); $x = 1$ (squares); $x = 5$ (diamonds). The solid lines are fits to the Gaussian distribution.

$$Q(a_m) \propto \exp\left[-\frac{1}{2}\left(\frac{a_m - a_0}{s_a}\right)^2\right] \tag{15}$$

where a_0 is the most probable radial semi-axis, and s_a is the corresponding width parameter. Distributions of the maximum polar semi-axis are defined analogously. The Gaussian function produced excellent fits to all of the DHS state-points and cavity elongations studied; results for $\rho^* = 0.2$ and $\mu^* = 2$ are included in Fig. 1. In Figs. 2, 3, and 4 we show the fitting parameters for DHS solvents at densities of $\rho^* = 0.2$, $\rho^* = 0.5$, and $\rho^* = 0.8$, respectively, as functions of the spheroid elongation. These figures also include the corresponding parameters for the polar semi-axis, c.

The results for $\rho^* = 0.2$ (Fig. 2) show that with all dipole moments, the most probable radial (polar) semi-axis decreases (increases) with increasing elongation. In addition, the most probable polar semi-axis for prolate cavities with elongation $x > 1$ is greater than the most probable radial semi-axis for oblate cavities with elongation $1/x < 1$; this is just due to fact that the polar semi-axis of a long, thin spheroid is longer than the radial semi-axis of a short, fat spheroid with the same volume. For a given cavity elongation, a_0 and c_0 are almost independent of the solvent polarity (except at the highest elongations considered where small deviations are apparent). The width parameters in the Gaussian functions vary in a similar way to the corresponding most probable values, although they appear to be more sensitive to the solvent dipole moment. Results for $\mu^* = 0$ and $\mu^* = 1$ are almost identical, but those for $\mu^* = 2$ are significantly larger for both semi-axes and all elongations. At low dipole moments (or high temperatures) the distribution of cavity sizes is narrower since there is only one characteristic lengthscale in the solvent. At high dipole

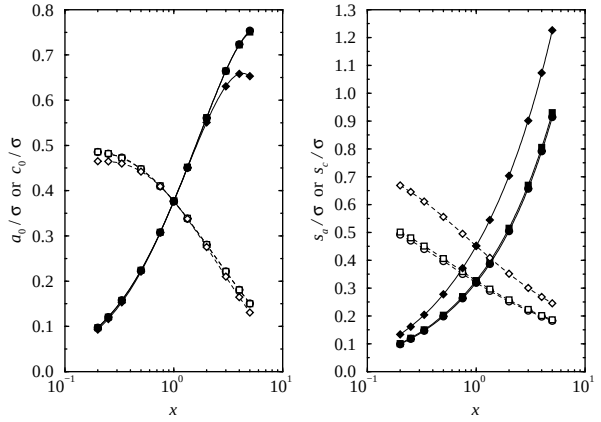

FIG. 2: Statistics for the radial semi-axis (open symbols) and polar semi-axis (filled symbols) of spheroidal cavities in DHS solvents at density $\rho^* = 0.2$ and dipole moments $\mu^* = 0$ (circles), $\mu^* = 1$ (squares), and $\mu^* = 2$ (diamonds): (left) most probable values, a_0 and c_0; (right) width parameters, s_a and s_c. Error bars are smaller than the symbols.

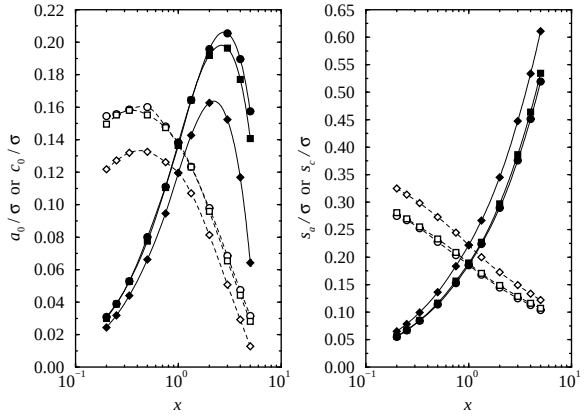

FIG. 3: Statistics for the radial semi-axis (open symbols) and polar semi-axis (filled symbols) of spheroidal cavities in DHS solvents at density $\rho^* = 0.5$ and dipole moments $\mu^* = 0$ (circles), $\mu^* = 1$ (squares), and $\mu^* = 2$ (diamonds): (left) most probable values, a_0 and c_0; (right) width parameters, s_a and s_c. Error bars are smaller than the symbols.

moments there is strong association of the solvent particles which gives rise to two structural lengthscales: the average distance between nearest-neighbor solvent particles, and the characteristic lengthscale of the cluster network.[22] This gives rise to a heterogeneous cavity structure in which small cavities are located in the vicinity of clustered solvent particles, and larger voids are formed in the free space between clusters. Hence, a broader distribution of cavity sizes is found at higher dipole moments. The width parameter is clearly a sensitive probe of the solvent structure.

Results for $\rho^* = 0.5$ (Fig. 3) and $\rho^* = 0.8$ (Fig. 4) show similar trends, except that the most probable dimensions show local maxima in the range of elongations considered. For a given solvent dipole moment, these maximal values of a_0 and c_0 occur for less anisotropic shapes as the density is increased, which suggests that there are fewer long 'holes' in the fluid structure at high densities. The most probable cavity dimensions and associated width parameters decrease with increasing density. This is because as the density is increased, the free volume in the vicinity of the clustered solvent molecules represents a greater proportion of the total free volume; since small cavities are located in the region of the solvent molecules, and large cavities are accommodated in the voids of the clustered network structure, the average cavity dimensions and associated 'standard deviations' will be reduced. a_0 and c_0 decrease with increasing solvent dipole moment, whereas s_a and s_c increase, once again due to the promotion of solvent-particle association. The development of a heterogeneous fluid structure gives rise to a greater spread of cavity sizes, whereas the shifts in a_0 and c_0 must be due to the decreasing nearest-neighbor separation between solvent particles.

The influences of solvent dipole moment on the fit parameters are seen to decrease in magnitude with increasing density. This is due to the fact that at low densities strongly interacting DHSs associate to form networks that possess heterogeneous cavity structures, whereas at high densities the fluid structure is not qualitatively different from that of pure hard spheres. This statement is backed up by Fig. 5, which shows the static structure factor, $S(q)$, in DHS solvents at each density and dipole moment considered in this work. There are many alternative choices of structural probe, but $S(q)$ does have the merit of observing certain characteristic scaling laws in the presence of strong particle association.[22] $S(q)$ was

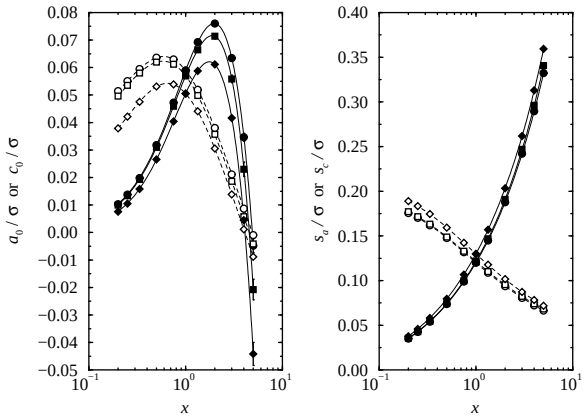

FIG. 4: Statistics for the radial semi-axis (open symbols) and polar semi-axis (filled symbols) of spheroidal cavities in DHS solvents at density $\rho^* = 0.8$ and dipole moments $\mu^* = 0$ (circles), $\mu^* = 1$ (squares), and $\mu^* = 2$ (diamonds): (left) most probable values, a_0 and c_0; (right) width parameters, s_a and s_c. Error bars are smaller than the symbols.

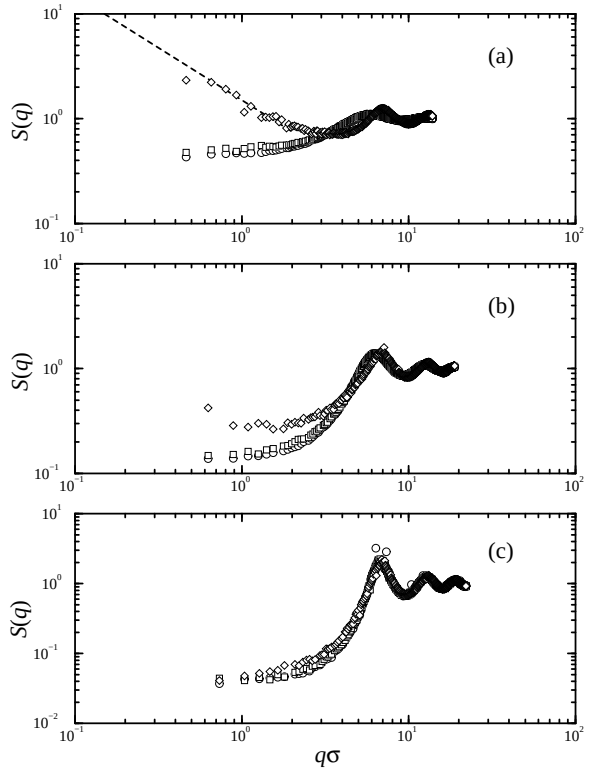

FIG. 5: Log-log plots of the static structure factors, $S(q)$, for DHS solvents with dipole moments $\mu^* = 0$ (circles), $\mu^* = 1$ (squares), and $\mu^* = 2$ (diamonds): (a) $\rho^* = 0.2$; (b) $\rho^* = 0.5$; (c) $\rho^* = 0.8$. The dashed line in (a) follows the power law $S(q) \propto q^{-1}$.

calculated in the simulations directly using the relation

$$S(\boldsymbol{q}) = \frac{1}{N}\left\langle \left[\sum_{i=1}^{N} \cos\left(\boldsymbol{q}\cdot\boldsymbol{r}_i\right)\right]^2 + \left[\sum_{i=1}^{N} \sin\left(\boldsymbol{q}\cdot\boldsymbol{r}_i\right)\right]^2 \right\rangle \tag{16}$$

where $\boldsymbol{q}$ is a reciprocal lattice vector of the simulation cell, and contributions with equal $q = |\boldsymbol{q}|$ were averaged. At a density of $\rho^* = 0.2$ the structure of the system with $\mu^* = 2$ is clearly different from the structures of those systems with $\mu^* = 1$ and $\mu^* = 0$. In particular, the strongly polar system exhibits power-law behavior at low q; as discussed fully in Ref. 22, chain-like correlations give rise to the scaling $S(q) \sim q^{-1}$. At the higher densities, the structural features of the fluid are far less sensitive to the dipole moment.

B. Parametrizing the SPT

To test the SPT expression in (11) we need to determine the values of the solute-solvent interfacial tension and the solvent equation of state. The latter was obtained as described in Section II D, and the results are included in Table II. The interfacial tension was obtained by fitting (11) to simulation results for spherical solutes only, with the intention of then applying the parametrized equation to non-spherical solutes. As examples of the procedure, in Fig. 6 we show the excess chemical potentials of hard-sphere solutes as functions of the radius, a, in DHS systems with $\mu^* = 2$. It is emphasized that the only fitting parameter in (11) is the reduced interfacial tension $\gamma\sigma^2/k_BT$.[36] The fits included in Fig. 6 are seen to be quite good, and the resulting fit parameters are reported in Table II. In earlier works,[10,11] it has sometimes proven necessary to modify the interfacial term with a curvature correction, i.e. the third term on the right-hand side of (11) is replaced by a contribution like[33]

$$\frac{\gamma S_2}{k_BT}\left(1 - \frac{4\delta}{R_2}\right) \tag{17}$$

where δ is also to be parametrized against simulation results. This modification was fully tested against simulation results, but in some cases it led to negative interfacial tensions, and in every case gave rise to significant uncertainties in the fit parameters with no visible improvement over (11).

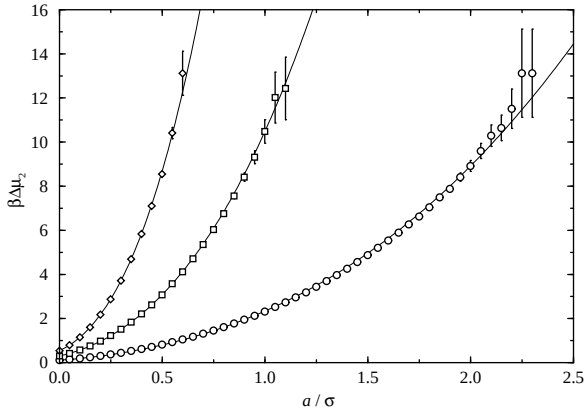

FIG. 6: Excess chemical potentials of hard-sphere solutes with radius a in DHS solvents with $\mu^* = 2$ and at various densities: $\rho^* = 0.2$ (circles); $\rho^* = 0.5$ (squares); $\rho^* = 0.8$ (diamonds). The symbols are from MC simulations and the curves are best fits using (11)

.

C. Excess chemical potentials of spheroid solutes

With (11) parametrized using simulation results for spherical solutes, we now turn to an examination of the excess chemical potentials for non-spherical solutes. To emphasize the effects of molecular shape we compare results for hard-spheroid solutes with the same volume, V_2, but with different elongations (and hence different R_2 and S_2). In Fig. 7 we present simulation results for DHS solvents at $\rho^* = 0.2$, and solutes with molecular volumes in the range $V_1 \le V_2 \le 20V_1$. For a given molecular volume the spherical solute has the lowest value of $\beta\Delta\mu_2$,

TABLE II: Thermodynamic properties of the DHS fluid: the reduced density ρ^*; the reduced dipole moment μ^*; the reduced temperature T^*; the radial distribution function at contact $g(\sigma)$; the dipolar energy, U, per molecule in units of k_BT; the reduced pressure $p\sigma^3/k_BT$; the reduced solute-solvent interfacial tension $\gamma\sigma^2/k_BT$.

ρ^*	μ^*	T^*	$g(\sigma)$	U/Nk_BT	$p\sigma^3/k_BT$	$\gamma\sigma^2/k_BT$
0.2	0	∞	1.3220	0	0.3107	0.13103(2)
0.2	1	1	1.6492	−0.2847	0.2812	0.13085(2)
0.2	2	0.25	9.6583	−4.6588	0.0774	0.09579(7)
0.5	0	∞	2.1558	0	1.6288	0.5128(1)
0.5	1	1	2.4148	−0.6625	1.4332	0.5089(1)
0.5	2	0.25	5.6678	−5.7950	0.5702	0.4516(1)
0.8	0	∞	4.0094	0	6.1742	1.3653(3)
0.8	1	1	4.2377	−1.0056	5.6758	1.3623(6)
0.8	2	0.25	6.1733	−6.8986	3.5558	1.3153(4)

and hence from (4) the highest solubility. This reflects the well-known fact that the ratio of surface area to volume is smallest for spherical molecules, and hence the unfavorable interfacial tension term in (11) is minimized with this geometry. $\beta\Delta\mu_2$ increases sharply as the solute geometry deviates from the sphere, and there is an approximate correspondence between the excess chemical potentials of oblate solutes with elongation $1/x < 1$ and prolate solutes with elongation $x > 1$, although at more extreme solute volumes the values for prolate solutes are clearly lower than those for the corresponding oblate solutes. These variations are well described by the SPT prediction (11) even though it was parametrized against spherical solutes only. Hence we conclude that the variations in $\beta\Delta\mu_2$ are mainly due to a combination of differences in the mean radius of curvature R_2, and the surface area S_2. This is illustrated in Fig. 8 which shows R_2 and S_2 as compared to the corresponding measures of spherical particles of the same volume. S_2/R_2 increases with increasing particle volume, and so eventually the variation of $\beta\Delta\mu_2$ with x will mirror that of S_2 shown in Fig. 8.

At higher densities very similar trends are observed in the results from simulations and SPT. Results for $\rho^* = 0.5$ and $\rho^* = 0.8$ are shown in Figs. 9 and 10, respectively. At $\rho^* = 0.5$ the simulation and SPT results clearly show that a prolate solute has a lower excess chemical potential than an oblate solute with reciprocal elongation and the same molecular volume. This trend is not obvious in the simulation results at $\rho^* = 0.8$ because we were only able to carry out calculations for $V_2 = V_1$ (although the SPT predictions for larger solute volumes will of course show this effect). Other trends apparent in Figs. 7, 9, and 10 include the increase in $\beta\Delta\mu_2$ with molecular volume and, more significantly, the decrease in $\beta\Delta\mu_2$ with increasing μ^* or decreasing T^*. Hence, the model system correctly shows that the solubilities of non-polar solutes in polar solvents (or at least those that can be described faithfully with a DHS model) will decrease with increasing temperature. This variation implies that $\partial \ln K/\partial T^* < 0$, and hence that the energy change $\Delta u_2 < 0$ (5). Since $\partial(T^* \ln K)/\partial T^* < 0$, it is

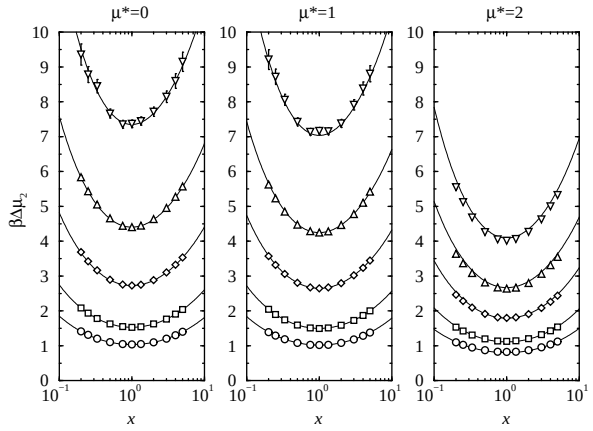

FIG. 7: Excess chemical potentials of hard-spheroid solutes with elongation x in DHS solvents with $\rho^* = 0.2$ and various dipole moments: (left) $\mu^* = 0$; (middle) $\mu^* = 1$; (right) $\mu^* = 2$. In each case the symbols correspond to solute molecular volumes of $V_2 = V_1$ (circles), $V_2 = 2V_1$ (squares), $V_2 = 5V_1$ (diamonds), $V_2 = 10V_1$ (up triangles), and $V_2 = 20V_1$ (down triangles). The symbols are from MC simulations and the curves are the predictions of (11).

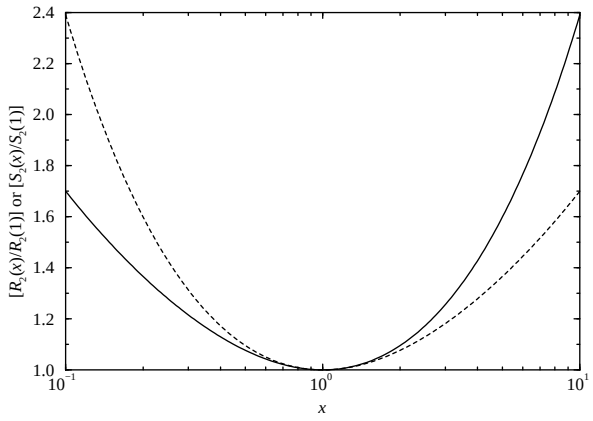

FIG. 8: Fundamental measures of spheroids compared to the corresponding measures of spheres with equal volume, as functions of the elongation x: the mean radius of curvature, R_2 (solid line); the surface area, S_2 (dashed line).

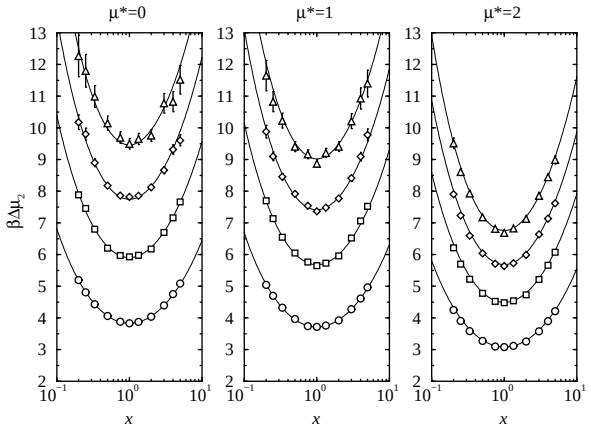

FIG. 9: Excess chemical potentials of hard-spheroid solutes with elongation x in DHS solvents with $\rho^* = 0.5$ and various dipole moments: (left) $\mu^* = 0$; (middle) $\mu^* = 1$; (right) $\mu^* = 2$. In each case the symbols correspond to solute molecular volumes of $V_2 = V_1$ (circles), $V_2 = 2V_1$ (squares), $V_2 = 3V_1$ (diamonds), and $V_2 = 4V_1$ (up triangles). The symbols are from MC simulations and the curves are the predictions of (11).

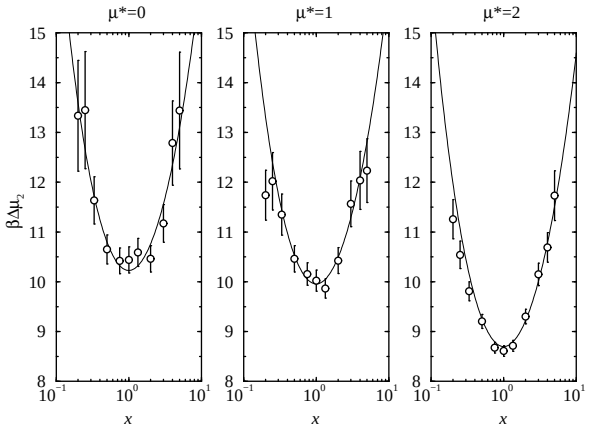

FIG. 10: Excess chemical potentials of hard-spheroid solutes with elongation x and molecular volume $V_2 = V_1$ in DHS solvents with $\rho^* = 0.8$ and various dipole moments: (left) $\mu^* = 0$; (middle) $\mu^* = 1$; (right) $\mu^* = 2$. The symbols are from MC simulations and the curves are the predictions of (11).

also clear that the entropy change $\Delta s_2 < 0$ (6). The magnitudes of the variations in $\beta\Delta\mu_2$ with temperature – and hence $|\Delta u_2|$ and $|\Delta s_2|$ – increase with increasing solute molecular volume. These results are analogous to those for hydrophobic solvation, in which the presence of a solute molecule in the solvent causes some sort of ordering of nearby solvent molecules with an associated decrease of the solvent-solvent interaction energy. It should be emphasized that in the present case, there are no solute-solvent interactions beyond the hard-core repulsion, and so an energy change upon inserting a solute molecule in to the DHS solvent would arise exclusively from solvent-solvent interactions. In contrast to real hydrophobic solvation, however, we anticipate that there will be no temperature minimum in the solubility; the hard-core repulsions between model solutes and solvents are never small compared to the thermal energy, and so $\beta\Delta\mu_2$ will level off asymptotically to the values presented here for the systems with $\mu^* = 0$.

IV. CONCLUSIONS

We have investigated the effects of molecular shape on the solvation of hard-core solutes in model polar solvents. The solutes are hard spheroids with a range of elongations and molecular volumes, while the solvent consists of a fluid of dipolar hard spheres. Although these are very crude representations, the properties of the model systems should bear some qualitative resemblance to those of real solutions.

Using computer simulations we have calculated the distributions of transient spheroidal cavities with specific elongations in the pure model solvents. For a given solvent molecular dipole moment, the most probable cavity dimensions decrease with increasing solvent density reflecting the reduction in free volume. More interestingly, for oblate spheroidal cavities the shape corresponding to the maximum average radial semi-axis become less anisotropic with increasing solvent density; the same is true for prolate spheroidal cavities with respect to the maximum average polar semi-axis. This suggests that at high solvent densities, the probability of developing a non-spherical cavity is reduced due to tight packing of the solvent molecules. For a given solvent density and cavity elongation, the average cavity size decreases with increasing solvent dipole moment (or decreasing temperature) due to the association of solvent particles and hence a reduction in the nearest-neighbor separation.

The excess chemical potentials of hard-spheroid solutes of various molecular volumes have been calculated; these are related to the cavity distributions since there is no solute-solvent interaction beyond the hard-core repulsion. For given solute molecular volume, solvent density, and temperature, the excess chemical potential is minimized for spherical solutes, while this function is less for a prolate solute with elongation x than it is for an oblate solute with elongation $1/x$. These observations are easily explained with reference to a simplified scaled-particle theory written in terms of the equation of state of the pure solvent, the solute-solvent interfacial tension, and fundamental measures of the solute molecule, i.e., the mean radius of curvature, the surface area, and the molecular volume. Firstly, the unfavorable interfacial tension contribution is minimized for spherical solutes. Secondly, the violation of $x \leftrightarrow 1/x$ symmetry for a given molecular volume is due to the differences in the mean radius of curvature and surface areas between the two shapes. Since the solubility of a spheroidal particle is simply related to the excess chemical potential, we can

predict that for a given molecular volume, rod-like particles should be more soluble than plate-like particles, and spherical particles should be the most soluble. To illustrate the magnitude of this effect, consider a DHS solvent with $\rho^* = 0.8$ and $\mu^* = 1$, which roughly corresponds to a typical polar molecular liquid. For prolate and oblate solutes with moderate elongations of 3 and 1/3, respectively, and with molecular volumes equal to that of a single solvent molecule, Eqs. (4) and (11) with the values given in Table II predict that the solubility of the prolate solute will be about 17% higher than that of the oblate solute. Doubling the solute volume would result in the prolate molecule being approximately 35% more soluble than the oblate one.

For given solute elongation and solvent density, the excess chemical potentials of the solutes increase with increasing molecular volume, and decrease with increasing solvent polarity (or decreasing temperature). The former trend is obvious, while the latter trend is due to the concentration of free volume mentioned above. The decrease in solubility with increasing temperature is similar to that observed in the solvation of hydrophobic solutes in water, and reflects the fact that the entropy of solvation is negative, i.e., the presence of the solute molecule would lead to an ordering of the solvent. As a result of this enhanced ordering, the energy change is also negative. In the present calculations, the negative energy change is entirely due to solvent-solvent interactions.

Unfortunately, a rigorous test of the simulation and theoretical results against experimental data is not yet feasible due to the restricted set of available molecular geometries and sizes; the key results presented here concern hard solutes of equal volume and with reciprocal aspect ratios. It would therefore be interesting to examine experimentally the solubilities of, for example, nanoscopic colloidal particles with well controlled geometries and particle volumes that are large compared to the solvent so that the prolate-oblate asymmetry is enhanced.

---

* E-mail:philip.camp@ed.ac.uk

[1] B. Widom, P. Bhimalapuram, and K. Koga, Phys. Chem. Chem. Phys. **5**, 3085 (2003).
[2] R. A. Pierotti, J. Phys. Chem. **67**, 1840 (1963).
[3] R. A. Pierotti, J. Phys. Chem. **69**, 281 (1965).
[4] M. Lucas, J. Phys. Chem. **80**, 359 (1976).
[5] L. R. Pratt and D. Chandler, J. Chem. Phys. **67**, 3683 (1977).
[6] K. Lum, D. Chandler, and J. D. Weeks, J. Phys. Chem. B **103**, 4570 (1999).
[7] L. R. Pratt, Annu. Rev. Phys. Chem. **53**, 409 (2002).
[8] B. Lee, Biopolymers **24**, 813 (1985).
[9] B. Lee, J. Chem. Phys. **83**, 2421 (1985).
[10] A. Pohorille and L. R. Pratt, J. Am. Chem. Soc. **112**, 5066 (1990).
[11] L. R. Pratt and A. Pohorille, Proc. Natl. Acad. Sci. USA **89**, 2995 (1992).
[12] L. E. S. de Souza, A. Stamatopoulou, and D. Ben-Amotz, J. Chem. Phys. **100**, 1456 (1994).
[13] L. E. S. de Souza and D. Ben-Amotz, J. Chem. Phys. **101**, 9858 (1994).
[14] A. Stamatopoulou, L. E. S. de Souza, D. Ben-Amotz, and J. Talbot, J. Chem. Phys. **102**, 2109 (1995).
[15] A. Stamatopoulou and D. Ben-Amotz, J. Chem. Phys. **106**, 1181 (1997).
[16] A. Stamatopoulou and D. Ben-Amotz, J. Chem. Phys. **108**, 7294 (1998).
[17] I. P. Omelyan and D. Ben-Amotz, J. Mol. Liq. **92**, 3 (2001).
[18] J. J. Weis and D. Levesque, Phys. Rev. Lett. **71**, 2729 (1993).
[19] J. J. Weis and D. Levesque, Phys. Rev. E **48**, 3728 (1993).
[20] D. Levesque and J. J. Weis, Phys. Rev. E **49**, 5131 (1994).
[21] P. J. Camp, J. C. Shelley, and G. N. Patey, Phys. Rev. Lett. **84**, 115 (2000).
[22] P. J. Camp and G. N. Patey, Phys. Rev. E **62**, 5403 (2000).
[23] P. I. C. Teixeira, J. M. Tavares, and M. M. Telo da Gama, J. Phys.: Condens. Matter **12**, R411 (2000).
[24] T. Tlusty and S. A. Safran, Science **290**, 1328 (2000).
[25] A. Zilman, T. Tlusty, and S. A. Safran, J. Phys.: Condens. Matter **15**, S57 (2003).
[26] B. Huke and M. Lucke, Rep. Prog. Phys. **67**, 1731 (2004).
[27] K. Koga, P. Bhimalapuram, and B. Widom, Mol. Phys. **100**, 3795 (2002).
[28] T. Boublik, J. Chem. Phys. **53**, 471 (1970).
[29] G. A. Mansoori, N. F. Carnahan, K. E. Starling, and T. W. Leland, Jr., J. Chem. Phys. **54**, 1523 (1971).
[30] H. Reiss, H. L. Frisch, and J. L. Lebowitz, J. Chem. Phys. **31**, 369 (1959).
[31] B. Widom, J. Chem. Phys. **39**, 2808 (1963).
[32] T. Kihara, Adv. Chem. Phys. **5**, 147 (1963).
[33] J. S. Rowlinson and B. Widom, *Theory of molecular capillarity* (Dover Publications, Inc., New York, 2003).
[34] M. P. Allen and D. J. Tildesley, *Computer simulation of liquids* (Clarendon Press, Oxford, 1987).
[35] J.-P. Hansen and I. R. McDonald, *Theory of simple liquids* (Academic Press, London, 1986).
[36] Note that in the particular case of the DHS solvent there is some uncertainty as to the location and nature of any vapor-liquid phase transitions and so γ cannot be approximated by a known surface tension. In any case, current estimates[21] of the 'critical temperature' correspond to reduced dipole moments of $\mu^* \simeq 2.5$ and so the solvents used here can be considered supercritical.